Nanoscale

PAPER

View Article Online
View Journal | View Issue



Cite this: *Nanoscale*, 2024, **16**, 16183

# Effect of NiAl alloy microparticles deposited in flexible SERS substrates on the limit of detection of rhodamine B molecules†

A. Molina,[a] J. Oliva, *[b] M. Vazquez-Lepe,[c] M. Lopez-Medina,[a] L. Ojeda,[a] D. Rios-Jara[a] and H. Flores-Zuñiga[a]

Received 22nd June 2024,
Accepted 25th July 2024

DOI: 10.1039/d4nr02592j

rsc.li/nanoscale

Flexible-SERS (FSERS) substrates were fabricated by depositing $Ni_{64}Al_{36}$(NiAl)-alloy-microparticles and/or spherical Ag-NPs (sizes of 10–40 nm) on recycled plastics, which had an aluminum layer on their surface. First, FSERS substrates made of Al + Ag-NPs and an area of 1 $cm^2$ were used to detect rhodamine B (RhB) molecules. The limit-of-detection (LOD) for RhB was $8.35 \times 10^{-22}$ moles (~503 molecules), and the enhancement factor (EF) was $3.11 \times 10^{15}$. After adding NiAl-microparticles to the substrate, the LOD decreased to $8.35 \times 10^{-24}$ moles (~5 molecules) and the EF was increased to $2.05 \times 10^{17}$. Such EF values were calculated with respect to substrates made only with Al + NiAl-alloy (without Ag-NPs), which did not show any Raman signal. Other FSERS substrates were made with graphene-layer + Ag-NPs or graphene-layer + NiAl-alloy + Ag-Nps, and the best LOD and EF values were $8.35 \times 10^{-22}$ moles and $6.89 \times 10^{15}$, respectively. Overall, combining the Ag-NPs and NiAl-alloy microparticles allowed for the zeptomole detection of RhB. This was possible due to the formation of Ag aggregates around the alloy microparticles, which enhanced the number of hotspots. If no alloy is present in the FSERS substrates, the detection of RhB is lowered. Overall, we presented a low-cost FSERS substrate that does not require expensive Au films or Au-NPs (as previously reported) to detect RhB at the zeptomole level.



## 1. Introduction

Currently, there is tremendous contamination of water sources due to agricultural and industrial activities. It is estimated that 300–400 megatons of waste are generated by populations worldwide, which contaminates rivers and oceans.[1] Such contaminated water sources and wastewaters (generated by houses and buildings) are processed by water treatment/desalination plants to produce clean water, which can be used by people in the kitchen or bathroom. However, most of these water treatment plants cannot eliminate traces of contaminants coming from pharmaceuticals, dyes or herbicides.[2] For this reason, it is necessary to utilize traditional techniques such as liquid-chromatography, electrophoresis, and absorbance to identify traces of contaminants. However, such methods involve long times of processing and complexity and are expensive.[3] However, surface-enhanced Raman spectroscopy (SERS) is a versatile, efficient, fast, and eco-friendly technique for finding traces of chemical compounds. Detection by SERS (enhancement of the Raman signal) is possible due to the electromagnetic enhancement, which is provoked by the surface plasmon resonance of metal nanoparticles and the analyte (molecule to be detected).[3] Typical Raman substrates are made of metal films (Au, Ag, Cu, *etc.*) deposited on glass slides or silicon wafers and are rigid. These films are grown using complex and expensive methods such as thermal evaporation or chemical vapor deposition.[3] To facilitate the detection of analytes (contaminant molecules) on surfaces or fruits, flexible SERS (FSERS) substrates have emerged, which are fabricated on cellulose, polymer films, cotton fabrics or even adhesive tape. These substrates can be coupled on curved surfaces to take samples from them.[4] In addition, the FSERS substrates can be cut with different shapes and are considered a non-invasive sampling tool. FSERS have been used to monitor the water quality and to detect industrial dyes or chemicals in food (quality control).[4] Another advantage is their light weight and can be coupled to portable devices such as cell phones or displays.[3] Typically, Ag and Au nanoparticles (NPs) have been used in FSERS substrates for the detection of noxious compounds.[2] For example, Ag nanocubes have been embedded in

[a]*División de Materiales Avanzados, Instituto Potosino de Investigación Científica y Tecnológica A. C., 78216 San Luis Potosí, SLP, Mexico*
[b]*Centro de Física Aplicada y Tecnología Avanzada Universidad Nacional Autónoma de México, Boulevard Juriquilla 3001, 76230 Querétaro, Mexico.*
*E-mail: joliva@fata.unam.mx*
[c]*Departamento de Ingeniería de Proyectos, CUCEI-Universidad de Guadalajara, Jalisco, Mexico*

† Electronic supplementary information (ESI) available. See DOI: https://doi.org/10.1039/d4nr02592j

polydimethylsiloxane (PDMS) membranes for the detection of methylene blue and Rhodamine 6G (textiles contaminants) with detection limits of $10^{-10}$ M and $10^{-9}$ M, respectively.[5] The enhancement factor in this last research was ~ $3.43 \times 10^6$. FSERS substrates are made on flexible substrates of cellulose/papers, cotton buds, fabrics and polymers (PMMA, PET and polypropylene), which are decorated with Ag and/or Au NPs for the detection of drugs (cocaine and heroine), dyes (rhodamine 6G (R6g) and malachite green (MG)) and pesticides (thiram, thiabendazole and methyl parathion) with detection limits of $10^{-6}$–$10^{-12}$ M.[4] Despite the high sensitivity of the FSERS substrates to detect contaminant molecules, they still present the following disadvantages: (1) they are expensive because nanolithography or complex printing techniques are needed to fabricate nano/micro structures, which can generate the Raman enhancement; (2) they still utilize expensive metals such as gold; and (3) the FSERS are made on expensive plastics, such as polyimide and PVDF, which contaminate the environment at the end of their lifetime. Consequently, it is necessary to find new ways to fabricate FSERS substrates at a low cost using fast fabrication methods.

To fabricate FSERS substrates at a low cost, we utilized a flexible plastic substrate (recycled from single-use packets) as a mechanical support for active nanomaterials. Single-use packets are massively wasted worldwide by restaurants and homes, producing contamination in the environment. Plastic pollution is currently a global problem because oceans and rivers are currently contaminated by microplastics made of polyethylene (PE), polypropylene (PP), *etc.*, affecting human health. The contamination of water sources by microplastics is unstoppable because the transition to sustainable packaging in the food and beverage industries is slow and expensive.[6] Thus, in this investigation, we employed recycled plastic substrates to palliate the problem of contamination produced by plastics. Rhodamine B (RhB) is selected as the analyte to be detected by our FSERS substrates because it is a toxic dye widely used in the textile/plastic industries and produces carcinogenic/neurotoxic effects for humans. This dye has been found in concentrations from ng to mg in wastewater processed in water treatment plants.[7] It has been reported that SERS substrates are applied for the detection of RhB or for a similar rhodamine (R6G) using the following combinations of materials: (1) dendritic copper nanoleaves deposited on $RbCu_4Cl_3I_2$ films, which had a limit of detection (LOD) of $10^{-13}$ and an enhancement factor (EF) of $3.6 \times 10^{10}$;[8] (2) 3D porous γ-$Fe_2O_3$/N-rGO with LOD of $5 \times 10^{-7}$ M;[9] (3) flexible-graphene-sheets/Ag NPs with LOD of $10^{-12}$ M and EF = $10^8$;[10] (4) core–shell satellite structure Ag@$SiO_2$-Au nanoparticles/silicon-wafer with an LOD of $10^{-9}$ M and EF = $1.5 \times 10^4$;[11] (5) Au/graphene/Cu film with a LOD of $10^{-9}$ M for RhB and an enhancement factor of ~$10^6$;[12] and (6) Ag nanocubes/glass that allowed the detection of RhB with LOD of $10^{-10}$ M and an enhancement factor of $10^6$.[13] As observed, the lowest detection limit and EF for the SERS substrates made with Ag NPs or graphene are $10^{-12}$ M and $10^8$, respectively. To decrease the LOD even more and enhance the EF, we fabricated FSERS substrates on the aluminum side (inner part) of the single-use packets (recycled from mayonnaise packets). First, the Al layer was coated with NiAl alloy microparticles with sizes of 5–40 μm. Next, an ink of Ag nanoparticles (with sizes of 10–40 nm) was dropped on the alloy microparticles, decorating in this way their surface. Thus, the FSERS substrate was Al/NiAl@Ag-NPs. This one allowed the zeptomole detection ($10^{-24}$ moles) of RhB with EF = $10^{17}$. To study the effect of the type of substrate on the detection of RhB, another substrate was made with the configuration graphene/NiAl@Ag-NPs. In this case, the LOD was $10^{-22}$ moles of RhB and the EF was $10^{15}$. The EF obtained with the two substrates above is among the highest reported so far for the detection of RhB. Using a combination of NiAl alloy + Ag-NPs is even more effective for the detection of RhB (at the zeptomole level) than the combination of Si/Au-film/Au-NPs previously reported.[14] High EF values were obtained due to the formation of multiple hotspots in a limited area, and they were produced by the agglomerates of Ag NPs. Thus, such a combination above of Al + alloy + Ag or graphene + alloy + Ag avoids the utilization of the expensive Au metal for the detection of RhB. Furthermore, the FSERS substrates were constructed on single-use packets, which decreased their cost and made them more attractive for commercial applications.

## 2. Experimental

### 2.1 Synthesis of the NiAl alloy and Ag nanoparticles

The $Ni_{64}Al_{36}$ (NiAl) alloy was synthesized as follows: first, stoichiometric amounts of Ni and Al metal powders (purity > 99.9%) were mixed using an agata mortar. Later, this mixture of powders was deposited on a copper crucible, and this was melted at 1100 °C by arc melting. Ingots were obtained, and they were remelted five times to ensure their homogeneity. Finally, the ingots were ground to obtain a fine metallic powder. However, the Ag nanoparticles were synthesized using a procedure previously reported.[15] A certain amount of $AgNO_3$ (from Sigma Aldrich) was dissolved in 50 mL of distilled water. Next, 200 mg of citric acid was added to the mixture, and the whole solution was stirred for 30 min at 70 °C. After this, 0.5 g of $NaBH_4$ was added to the aqueous solution, and the silver nitrate was reduced to form Ag nanoparticles. The final solution had a dark-green coloration.

### 2.2. Fabrication of SERS substrates

The FSERS substrates were fabricated as follows: pieces of single-use packets (SUPs) were cut with dimensions of 2.7 cm × 2.2 cm and washed with alcohol/distilled water. Afterward, a slurry-paste was prepared by mixing polymethylmetacrylate, NiAl and acetone at a weight ratio of 0.25 : 0.35 : 1, respectively. Next, this slurry was deposited on the Al layer (gray side) in the SUPs using a bar-coating method and dried at 90 °C for 15 min. Later, 10 layers of Ag NPs were deposited on the side of an aluminum layer in the SUPs. For this, 300 μl of the Ag NPs (dark-green solution) was dropped on the Al layer, and this was dried at 90 °C for 5 min. This last procedure was repeated 10 times. This procedure produced the FSERS sub-

 

strates of Al/NiAl@Ag-NPs, which was named as AAAg (aluminum/alloy/Ag) substrate. The same procedure was utilized to make the FSERS substrates with graphene (G), but graphene was printed on the Al layer in the SUPs before the deposition of the NiAl alloy. For this purpose, the following process was employed. First, commercial graphene microplates (American Materials Co.), isopropyl-alcohol, acetone and sodium dodecyl sulfate were mixed (at a weight ratio of 0.6 : 1 : 1 : 0.15, respectively) by ultrasonication. Subsequently, the graphene ink was printed on the Al layer using the Blade method. The FSERS substrate made with graphene + alloy + Ag-NPs was named GAAg. Fig. S1 in the ESI† depicts a schematic illustration showing the architectures of the FSERS substrates utilized in this work. Fig. S1a† illustrates the FSERS substrate made of graphene, while that in Fig. S1b† illustrates that made of an Al layer (from a single-use packet).

### 2.3 Optical, morphological and structural characterization for the SERS substrates

Scanning Electron Microscopy (SEM) technique was employed to observe the morphology and microstructure of the FSERS substrates and alloy powders. This was carried out using FEI-ESEM Quanta 250 equipment with an electron beam at an energy of 5 keV. Additionally, Elemental Dispersion Spectroscopy (EDS) was used for elemental analysis with a ThermoFisher detector coupled with the SEM microscope. For the crystallographic identification of the alloys, graphene and Al, X-ray Diffraction (XRD) was used (SmartLab RIGAKU equipment). XRD scanning was performed at a speed of 0.1° $s^{-1}$ in the range of 10–80° at a Cu-kα wavelength of 1.5418 Å. X-ray photoelectron spectroscopy (XPS) spectra were acquired using a Thermo Scientific K-Alpha instrument. Fourier transform infrared (FTIR) spectroscopy was carried out using a Shimadzu spectrophotometer coupled to the ATR accessory (FTIR spectra were measured in the range of 400–4000 $cm^{-1}$). Finally, optical UV-Vis-NIR absorbance was determined using a Cary 5000 spectrophotometer.

### 2.4 Methodology for Raman measurements

First, molar solutions of RhB were prepared with concentrations ranging from $8.35 \times 10^{-5}$ to $8.35 \times 10^{-20}$ M. Later, 100 μl of each RhB solution was dropped on the AAAg and GAAg substrates. After this, they were analyzed using a micro-Raman Renishaw instrument (coupled to a green laser of 532 nm), and the Raman spectra were recorded in the range of 600–1800 $cm^{-1}$. A representative Raman spectrum was obtained by averaging 10 Raman curves measured at different points on the FSERS substrates. For all the Raman measurements, the spot size of the laser was ~7.75 μm, and the spot area was ~188.7 $\mu m^2$.

## 3. Results and discussion

### 3.1 Morphological, structural and optical characteristics of FSERS substrates

Fig. 1a shows an SEM image of the Al layer deposited on one of the sides (inner part) of the single-use packet. Such an

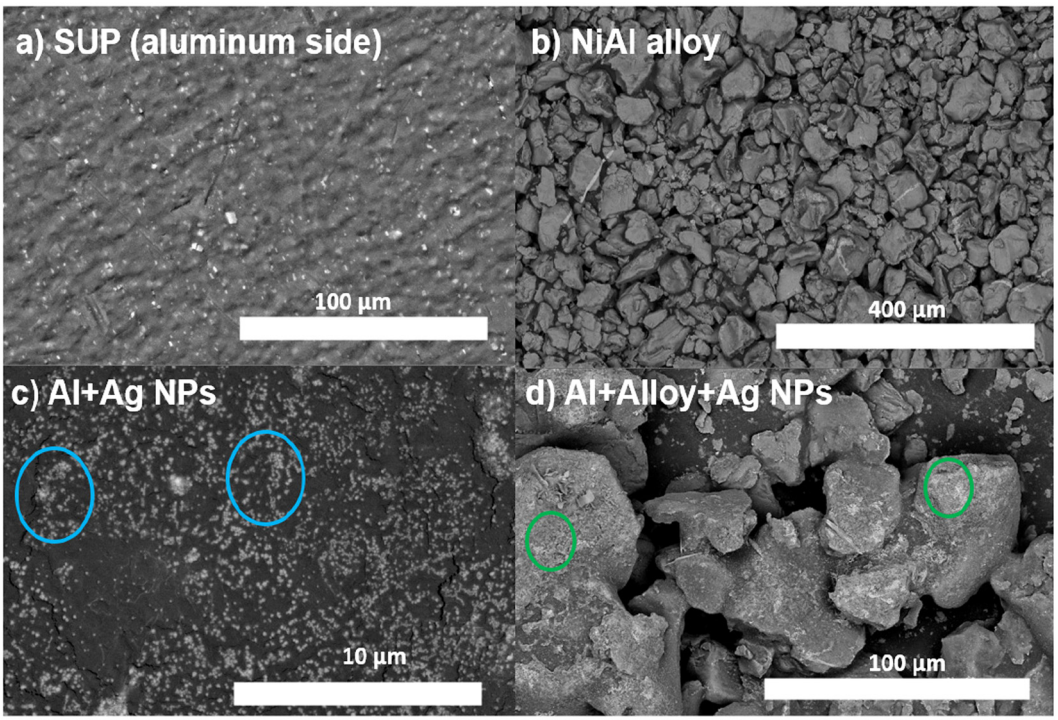


**Fig. 1** Micrographs (SEM images) for (a) aluminum layer on the single-use packet, (b) NiAl alloy microparticles, (c) FSERS substrate made with Al + Ag-NPs and (d) FSERS substrate made with Al + NiAl alloy + Ag-NPs.

aluminum layer is rough, and several polymer microparticles with irregular shapes are embedded in it. The NiAl alloy microparticles depicted in Fig. 1b have a rock-like morphology and, thus, an irregular shape. The smallest microparticles have sizes of 2–15 μm, and the biggest ones have sizes of 45–88 μm. Fig. 1c shows the SEM image for the Al layer coated with only the Ag nanoparticles. The Ag nanoparticles have a quasi-spherical shape and sizes of 10–40 nm and are conglomerated; see the blue circles. The biggest clusters are formed by 10–35 nanoparticles. The smallest clusters are formed by 3–12 nanoparticles; see the yellow circles in Fig. S2a in ESI.†

Fig. 1d shows the NiAl alloy microparticles decorated with Ag nanoparticles. In general, the alloy microparticles have irregular shapes and are compacted/overlapped. The green circles indicate the parts of the alloy microparticles decorated with Ag nanoparticles. A closer view of such alloy microparticles in Fig. S2b of the ESI† depicts the areas with Ag clusters on the NiAl alloy microparticles; see the orange circles.

However, the FSERS substrates made with graphene were also analyzed. Fig. 2a shows the bare graphene substrate where coalesced graphene microplates are observed. Such coalesced microplates have an average dimension of 7.8 μm × 13.3 μm and form a conductive surface with a sheet resistance of 12 ± 0.5 Ω $sqr^{-1}$. After depositing the Ag nanoparticles on the graphene substrate, they are homogeneously distributed (Fig. 2b). A zoom of the graphene substrate decorated with Ag nanoparticles did not show conglomerations of Ag nanoparticles (Fig. 2c). They only look like small dots distributed on the graphene microplates. Fig. 2d shows the arrangement of the NiAl alloy microparticles on the graphene substrate. These microparticles appear less compacted and more separated than the microparticles deposited on the Al substrate, as shown in Fig. 1d and 2d.

EDS analysis was also performed to confirm the elemental composition of the FSERS substrates. Fig. 3a shows the EDS spectrum for the FSERS substrate made with an aluminum layer covered by Ag NPs (the gray side of the SUPs was coated with Ag NPs, and this aluminum layer was deposited by the manufacturer of the SUPs). The energy peaks for the C and O elements are observed, which correspond to the polyethylene in the SUPs as well as the energy peaks for the Al and Ag elements. Fig. 3b shows the EDS spectrum for the FSERS substrate with Al + NiAl-alloy + Ag-NPs. In this case, the Ag nanoparticles decorated the aluminum substrate and alloy microparticles. An extra energy peak for the Ni element is shown in Fig. 3b due to the introduction of the NiAl alloy. Fig. 3c and d depict the EDS spectra for the FSERS substrate made with graphene (G) + Ag-NPs and graphene + alloy + Ag-NPs. As expected, these FSERS substrates had a much higher carbon component in comparison with the substrates made with the Al layer, compare, for example, Fig. 3a and c. The unique difference between the EDS spectra in Fig. 3c and d is the presence of Ni, which was observed only in the substrate made with graphene + alloy. In general, no additional chemical

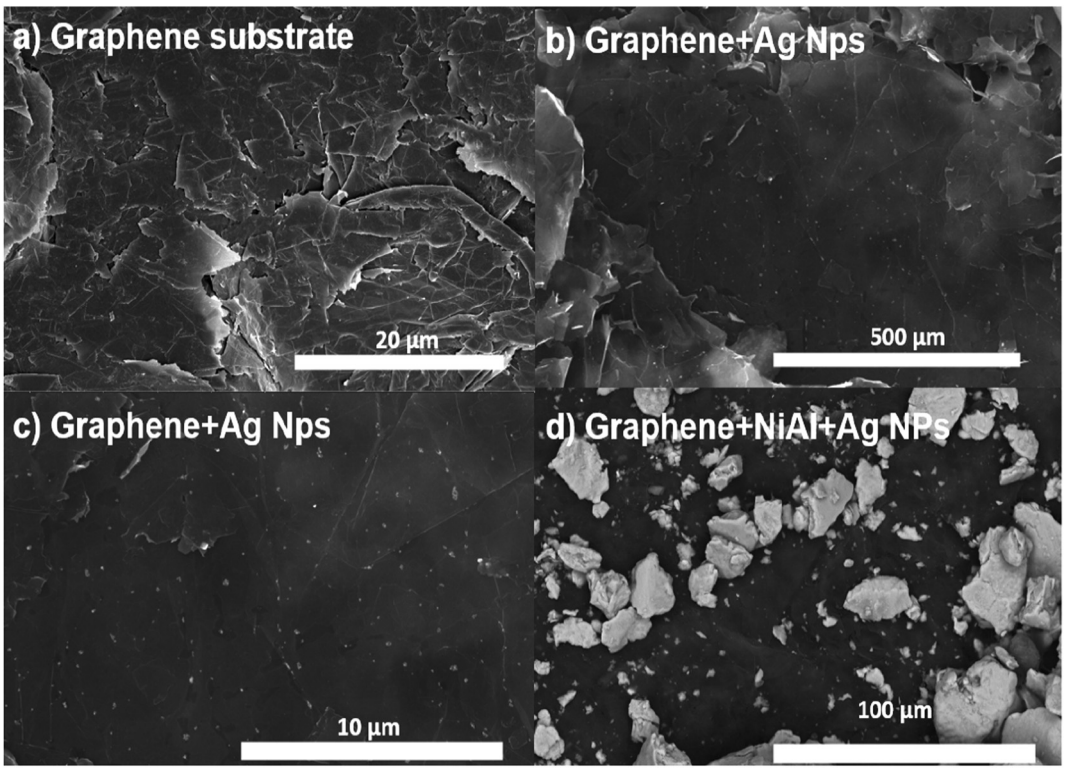


Fig. 2 Micrographs (SEM images) for (a) graphene layer deposited on the single-use packet, (b) and (c) are FSERS substrates made with G + Ag-NPs. (d) shows the FSERS substrate made with G + alloy + Ag-NPs.

 

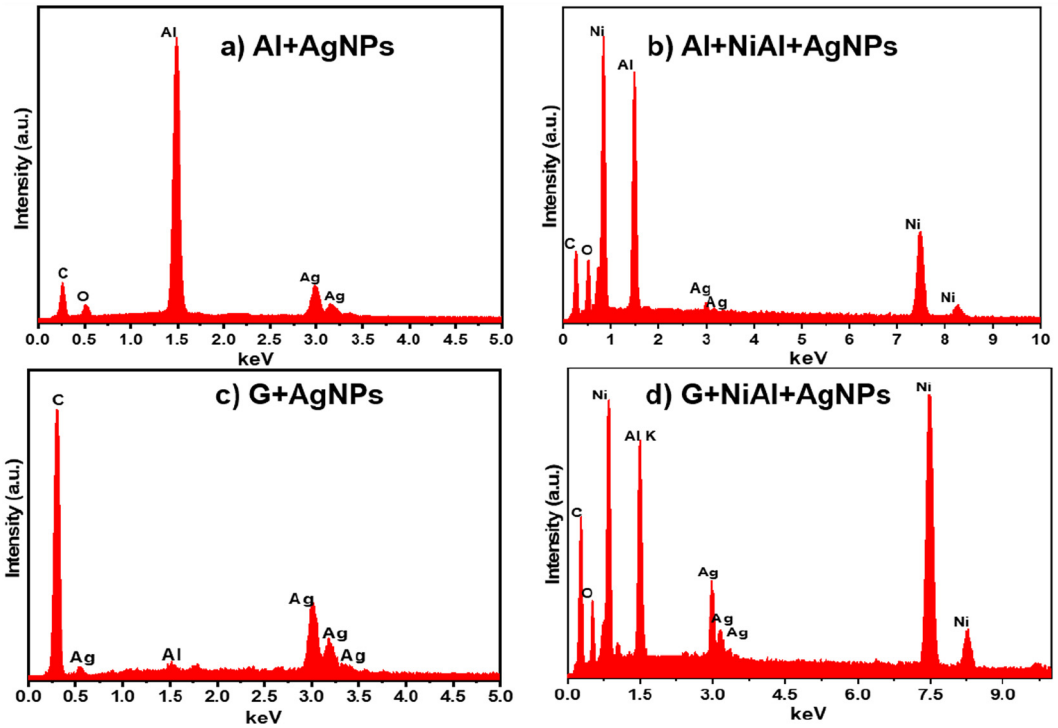


**Fig. 3** EDS spectra for the FSERS substrate made of (a) Al + Ag-NPs, (b) Al + alloy + Ag-NPs, (c) G + Ag-NPs and (d) G + alloy + Ag-NPs.

elements were observed in the EDS spectra of Fig. 3, confirming that our procedure is appropriate for fabricating FSERS substrates without impurities, which can affect Raman detection.

Fig. 4a shows the XRD pattern for the pure NiAl alloy powder. The most intense peak corresponds to the (111) orientation and cubic phase.[16] In the case of the XRD pattern of the Al layer printed in the single-use packet, the most intense peak corresponds to the (200) orientation and cubic phase[17] (Fig. 4b). The FSERS substrate of Al + alloy simultaneously shows the peaks of Al and the alloy; see the dotted lines in Fig. 4c. Interestingly, the XRD pattern for the FSERS substrate made of Al + Ag-NPs exhibited the (122), (231) and (241) orientations, which are attributed to the cubic phase of metallic Ag[18] (Fig. 4d).

The broad band observed at 22.5° is associated with the high-density polyethylene (HDPE) of the single-use packet.[19] Moreover, the FSERS substrate made of Al + alloy + Ag-NPs exhibited only the diffraction peaks for Al and NiAl (Fig. 4e). The diffraction peaks of silver were not observed because they were hidden by the high intensities of the Al and NiAl peaks. However, the FSERS substrate made with an Al layer coated with graphene (G) depicts an intense peak at 26.5°, which corresponds to the (200) orientation of graphene[20] (Fig. 4g). In addition, the FSERS substrate made with G + alloy exhibited the diffractions of graphene and NiAl simultaneously (compare the dotted lines in Fig. 4f and h), while the XRD pattern of the G + Ag substrate depicted the intense peak of graphene plus small peaks associated with metallic Ag (see (111), (200), (004) and (220) orientations in Fig. 4i). Finally, Fig. 4j shows that the FSERS substrate made of G + alloy + Ag-NPs is composed of the diffraction peaks of graphene, NiAl and Ag. Because the content of Ag is the lowest in that substrate, it is expected to be the lowest intensity peak for the Ag; see the peak for the (220) orientation in Fig. 4j.

### 3.2 Performance in the detection of RhB molecules

To evaluate the performance of the FSERS substrates for the detection of RhB molecules in an area of 1 $cm^2$ (or $1 \times 10^8$ $\mu m^2$), we first deposited on the Al substrate (gray side in the recycled single-use packet) 0.835 moles of RhB, but no Raman signal was produced; see the black curve in Fig. S3a in the ESI.† Subsequently, the NiAl alloy powder was deposited on the Al substrate. Next, two different concentrations of RhB were deposited (0.835 and $8.35 \times 10^{-9}$ moles) on the Al + alloy, but again, no Raman peaks were observed; see the red and blue curves in Fig. S3a.† This means that the Al layer and the combination of Al + alloy are not enough to produce the Raman signal. In the next step, the Al layer was coated with Ag NPs and deposited on this substrate RhB at a concentration of $8.35 \times 10^{-9}$ moles. Interestingly, Raman peaks were observed (Fig. 5a). These Raman peaks are very similar to those already reported in the literature for RhB.[21,22] Fig. 5a shows how the intensity of Raman peaks decreases after decreasing the RhB concentration on the FSERS substrate (Al + Ag-NPs) from $8.35 \times 10^{-9}$ moles to $8.35 \times 10^{-22}$ moles. A zoomed view of the Raman spectra for concentrations from $8.35 \times 10^{-16}$ to $8.35 \times 10^{-22}$ moles is shown in Fig. S4a of the ESI.† Fig. S1c† shows

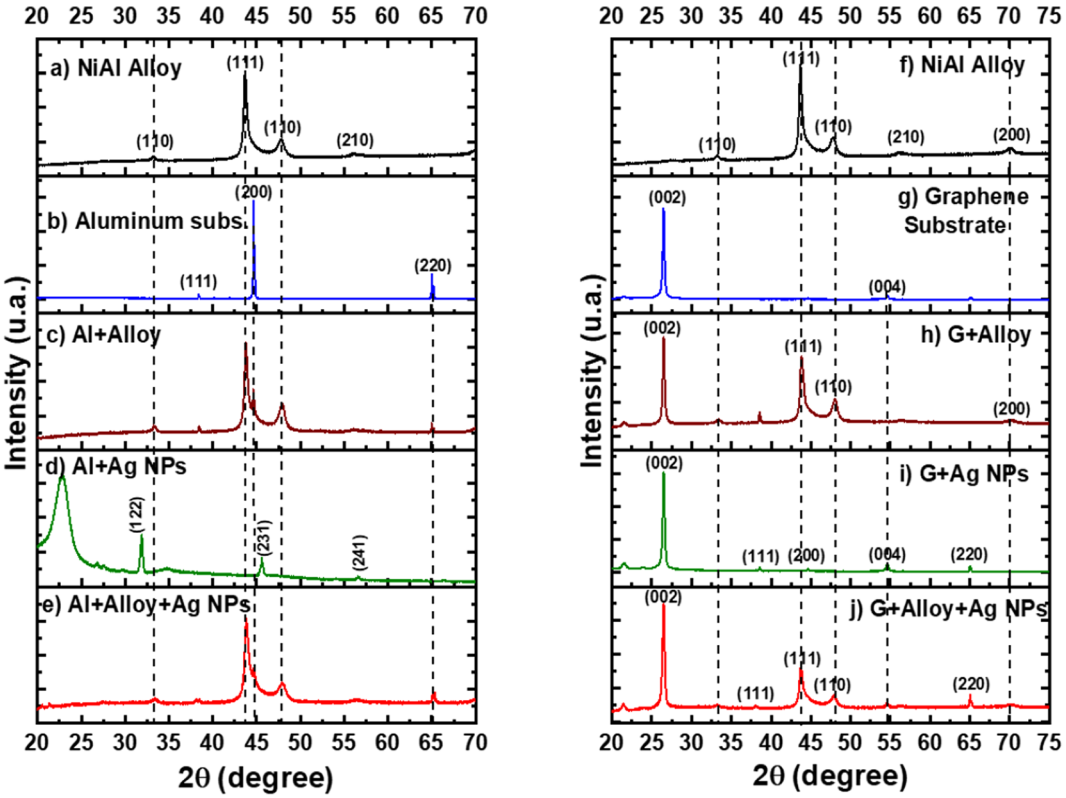


**Fig. 4** X-ray diffraction patterns for (a) NiAl powder, (b) Al layer, (c) Al + alloy, (d) Al + Ag-NPs, (e) Al + alloy + Ag-NPs, (f) NiAl alloy, (g) graphene substrate, (h) G + alloy, (i) G + Ag-NPs and (j) G + alloy + Ag-NPs.

pictures of the flexible Raman substrate fabricated in this study.

The Raman enhancement (also known as Enhancement factor = EF) was calculated for the detection of each RhB concentration using the following equation: $EF = [(I_{sers} \times N_{ref})/(I_{ref} \times N_{SERS})]$, where $I_{sers}$ is the intensity of the Raman peak obtained from the FSERS substrate with Ag NPs, $I_{ref}$ is the Raman signal obtained from the substrate without Ag NPs, $N_{ref}$ is the number of RhB molecules on the substrate without Ag NPs and $N_{SERS}$ is the number of RhB molecules on the substrate with Ag NPs. For the calculation of the enhancement factor, we used the integrated intensity of the Raman peak located at 1511 $cm^{-1}$ because it appeared in all the Raman spectra for the samples labeled as AlAg, AAAg, GAg and GAAg. Table S1 in the ESI† summarizes the concentration of RhB (in moles) for each FSERS substrate made with Al + Ag-NPs, the amount of RhB molecules on each SERS substrate, and their EF values. These EF values were calculated with respect to the following reference FSERS substrates: bare Al and Al + NiAl alloy did not produce Raman peaks, but they had $8.35 \times 10^{-9}$ moles of RhB on their surface. In particular, the AlAg-1 substrate had a Raman enhancement of 33 495 times with respect to these reference substrates. The AlAg-7 substrate (which had $8.35 \times 10^{-22}$ moles of RhB or ~503 molecules) showed a maximum EF value of $3.11 \times 10^{15}$. When the AlAg-1 sample is used as the reference substrate, the maximum EF value is now $1.07 \times 10^{11}$. Subsequently, FSERS substrates made with the configuration Al + NiAl alloy + Ag NPs were utilized to detect the same concentrations of RhB (~$10^{9}$ to $10^{-22}$). Surprisingly, the limit of detection (LOD) was even lower ($8.35 \times 10^{-24}$); see Fig. 5b and S4b in ESI.† This means that adding the NiAl alloy microparticles to the FSERS substrates decreases the LOD by two orders of magnitude. If the Raman spectra (at an RhB concentration of $8.35 \times 10^{-9}$ moles) in Fig. 5a and b are compared, it is clear that the Raman peaks observed in the substrate made with NiAl alloy are on average 214% more intense. For lower RhB concentrations (from ~$10^{-18}$ to ~$10^{-22}$ moles), the Raman peaks were also more intense for the substrates made with the NiAl alloy, compared with those in Fig. S4a and S4b in the ESI.† Furthermore, Table S1† illustrates that the FSERS substrate made with Al + alloy + Ag-NPs used to detect $8.35 \times 10^{-9}$ moles of RhB (AAAg-1) had ~78% more intense Raman peaks than the substrate made without alloys (AlAg-1). The maximum EF value produced by the FSERS substrates made with alloy was $2.05 \times 10^{17}$, which allowed the detection of $8.35 \times 10^{-24}$ moles of RhB or approximately 5 molecules; see Table S2 in the ESI.† When the AAAg-1 sample is used as a reference to calculate the EF value for the AAAg-8 sample, we obtained an EF value of $3.42 \times 10^{12}$. To evaluate the effect of the conductive film deposited on the FSERS substrate, we deposited graphene (G) microplates on the Al layer and then on the Ag NPS. The Raman spectra recorded from FSERS sub-

 

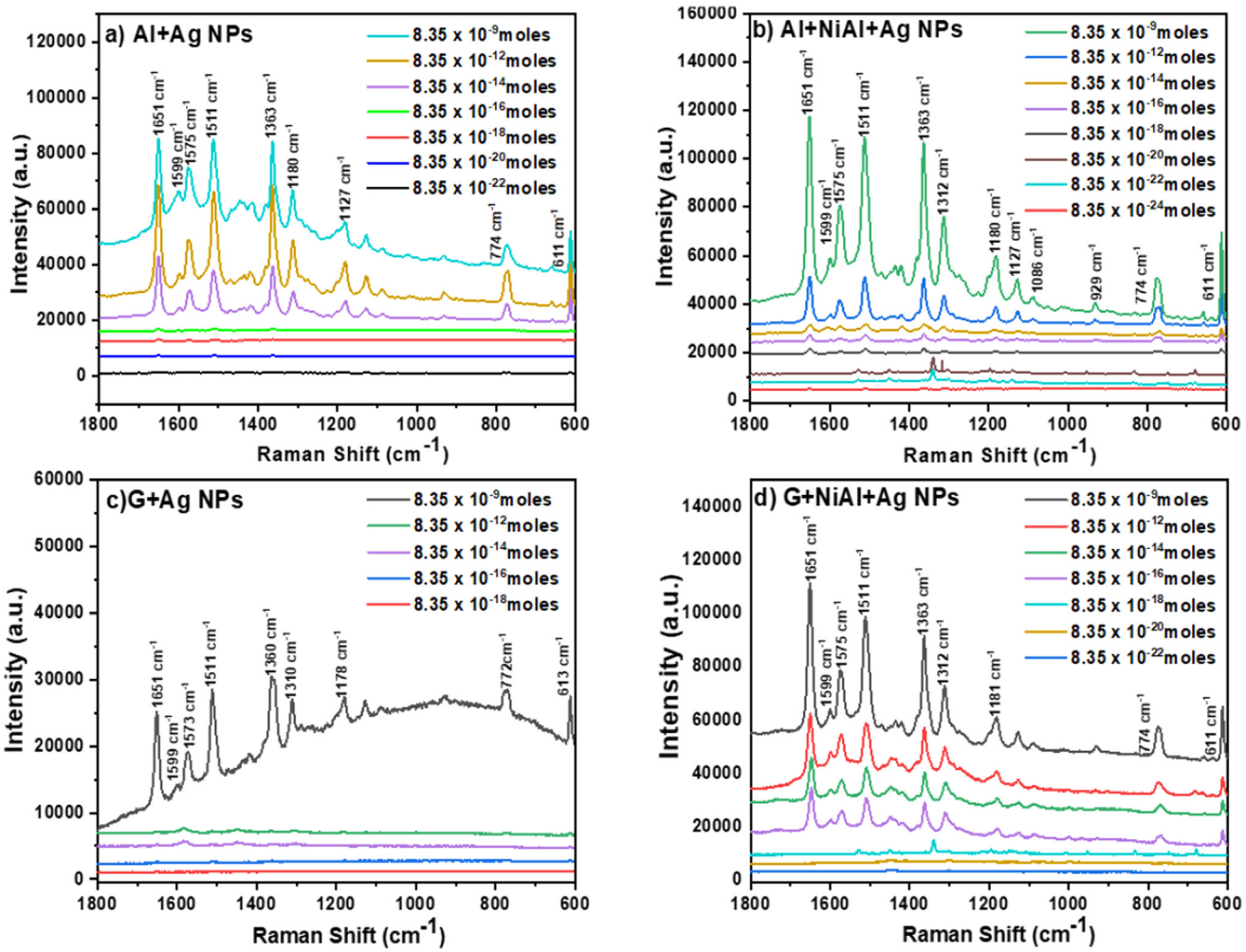


**Fig. 5** Raman spectra obtained for different RhB concentrations and using FSERS substrates made of (a) Al + Ag-NPs (AAg), (b) Al + alloy + Ag-NPs (AAAg), (c) G + Ag-NPs (GAg) and (d) G + alloy + Ag-NPs (GAAg).

strates made with pure graphene or G + alloy are exhibited in Fig. S3b of the ESI.† These substrates had $8.35 \times 10^{-9}$ moles of RhB on their surface, but no Raman peaks were observed. Later, other FSERS substrates were made with G + Ag-NPs, and different concentrations of RhB were deposited on their surfaces. The resulting Raman spectra for these substrates are shown in Fig. 5c. In this case, the LOD was only $8.35 \times 10^{-16}$ moles, that is, it was not possible to detect the lower concentration of RhB ($8.35 \times 10^{-18}$) because no Raman peaks were observed; see the red line in Fig. S4c in the ESI.† The maximum EF value for the substrates made with G + Ag-NPs was $2.7 \times 10^{9}$; see Table S3 in the ESI.† If the NiAl alloy is added to the FSERS made with graphene (G + AlNi + Ag-NPs substrates), it is possible to obtain stronger Raman peaks (Fig. 5d), and a lower LOD of $8.35 \times 10^{-22}$ moles for RhB is reached. This represents a maximum enhancement factor of $6.89 \times 10^{15}$; see Table S4 in the ESI.† A comparison between Fig. 5c and d indicates that adding the NiAl to the FSERS substrates increases the intensity of the Raman peaks on average 4.5 times for the Raman spectra corresponding to the concentrations of $10^{-9}$ moles. This is even evident at lower RhB concentrations; see the Raman peaks for $8.35 \times 10^{-14}$ and $8.35 \times 10^{-18}$ moles in Fig. S4c and S4d in the ESI.† By comparing the Raman spectra in Fig. 5, we infer the following facts: (i) RhB can be detected at the zeptomole level using the following combination of materials Al + Ag-NPs or G + NiAl + Ag-NPs; (ii) the ultimate detection level of $8.35 \times 10^{-24}$ moles (or ~5 molecules in 1 $cm^2$) is produced only in the FSERS substrates with Al + NiAl + Ag-NPs; (iii) in general, the Raman peaks are stronger in the FSERS substrates made with Al and (iv) the highest EF value of $10^{15}$–$10^{17}$ was obtained in the FSERS substrates made with NiAl alloy.

However, the EF values and the LOD obtained in this research were compared with others already reported in the literature for the detection of RhB using SERS substrates made with Ag NPs or graphene. For example, SERS substrates of $Ag_2CO_3$ microcrystals/glass produced a maximum EF = ~$10^6$, and the LOD was $10^{-11}$ M;[23] AuNP/AgNW composites/quartz could detect up to $10^{-15}$ M of RhB.[24] Another study employed SERS substrates made of Ag-NPs/reduced-graphene-oxide/glass

and detected a minimum concentration of $10^{-9}$ M, with an EF of $10^5$.[25] Additionally, SERS substrates made of Ag-NPs/Si/$SiO_2$ produced an EF of 35.4 for the detection of 2 μg of RhB.[26] Another study utilized Au-nanorods/melamine-foam as a SERS substrate and detected rhodamine with an LOD of $10^{-12}$ M (ref. 27) (the EF value was not reported). For comparison purposes, we should mention that a RhB solution $10^{-20}$ M was employed to take the five molecules of RhB deposited on the FSERS substrate. Thus, our LOD for the detection of RhB is at least 8 orders of magnitude lower than those reported in the literature (in terms of molar solutions). It is worth noting that our FSERS substrates have additional advantages over the previous SERS substrates: (i) our substrates were fabricated on recycled plastics, which significantly decreased their cost; (ii) our EF values ($10^{15}$–$10^{17}$) surpassed at least 5–7 orders of magnitude the EF values already reported in the literature for the detection of RhB; and (iii) we utilized an Al or graphene layer in the FSERS substrate instead of Au films or Si, which helped to decrease the cost of the substrate.

To analyze the reproducibility/stability of the FSERS substrates, several experiments were carried out: (1) first, two SERS substrates (made with Al + alloy + Ag-NPs and stored for 10 months) were taken, and $8.35 \times 10^{-9}$ moles or RhB was deposited on the first substrate (to make a new AAAg-1 sample). Next, $8.35 \times 10^{-24}$ moles of RhB were dropped on the second SERS substrate (to make a new AAAg-8 sample). After this, both substrates were analyzed using a Raman microscope. Their spectra are displayed in Fig. S5a and S5b.† If the Raman spectra in S5a† are compared with those in Fig. 5b made with $8.35 \times 10^{-9}$ moles, we observe the same Raman peaks, but the intensity of the new Raman peaks is on average 42% lower. In contrast, the comparison of the Raman spectra in Fig. S5b and S4b† for the samples made with $8.35 \times 10^{-24}$ moles of RhB revealed that the Raman intensity increased about 10 times. This confirmed that the SERS substrates are stable enough to be used after 10 months, and the Raman signals are obtained again. Even better, the Raman signal for the SERS substrate containing $8.35 \times 10^{-24}$ moles improved. (2) For the second experiment, we simply measured the Raman spectra for the old AAAg-1 and AAAg-8 samples (contained RhB), which were stored for 10 months (Table S1†) and recorded again the Raman spectra for such samples; see Fig. S6a and S6b in ESI.† As observed, the intensity of the Raman peaks for the AAAg-1 sample is on average 91% lower in comparison with the Raman spectra depicted in Fig. 5b (see the green curve for the concentration of $8.35 \times 10^{-9}$). In addition, the Raman peaks for the AAAg-8 sample were slightly stronger than those observed for the same sample in Fig. S4b of the ESI.† Thus, the same Raman peaks were obtained for the SERS substrates stored for 10 months; this was possible due to the high stability of the SERS substrates.

To prove the usefulness of flexible SERS substrates in detecting traces of RhB on curved surfaces, we performed experiments for RhB detection on apples. For this purpose, two apples were contaminated with RhB. The first apple was contaminated with RhB at a concentration of $8.35 \times 10^{-9}$ moles, and the second apple was contaminated with RhB at a concentration of $8.35 \times 10^{-18}$ moles (Fig. S7a†). Next, the layer of RhB deposited on the apple was dried naturally (Fig. S7b†). Subsequently, we put one AAAg (Al + NiAl + Ag-NPs) SERS substrate on the apple, as depicted in Fig. S7c,† to collect the RhB molecules. After this, the AAAg substrate was analyzed, and we obtained the Raman spectrum shown in Fig. S8a.† As observed, the Raman peaks are well defined, and their intensity is on average 75% lower than that obtained for the AAAG-1 substrate in Fig. 5b. It is expected to have a lower Raman intensity because only some of the RhB molecules were taken from the apple surface. A similar procedure was carried out using a second AAAg substrate, and the apple was contaminated with $8.35 \times 10^{-18}$ moles of RhB (this was the minimum detectable concentration of RhB on apples). The Raman spectrum for the second apple is presented in Fig. S8b† and well-defined peaks are again observed. Overall, it is possible to conclude that our flexible SERS substrates are useful for detecting traces of contaminants on curved surfaces. In fact, detecting contaminants in fruits is of particular interest to the food industry. Additionally, we demonstrated the effectiveness of our SERS substrates in detecting traces of other contaminants, such as herbicides. For this purpose, two AAAg substrates were fabricated, and 4-chlorophenol (4-CP) herbicide was deposited on them. 4-CP was selected because it is toxic for aquatic organisms, is persistent in the environment and can produce skin cancer in humans.[28] The first SERS substrate (AAAg-CP1) was contaminated with $8.35 \times 10^{-9}$ moles of 4-CP, and the second one (AAAg-CP2) was contaminated with $8.35 \times 10^{-16}$ moles of 4-CP. Subsequently, the Raman spectra were measured for such substrates; see Fig. S9 in the ESI.† From this last figure, it is observed that the intensity of the Raman peaks for the AAAg-CP2 substrate is on average 75% lower than those for AAAg-CP1. In fact, the lowest detectable concentration for 4-CP was $8.35 \times 10^{-16}$ moles. The EF for the AAAg-CP2 substrate (taking as reference the AAAg-CP1 substrate) was $2.53 \times 10^6$.

### 3.3 Mechanism for the detection of RhB molecules

To explain the high EF values, we first consider the absorption of light by each component on the FSERS substrates. Fig. 6a depicts the absorbance spectra for the Al layer (gray side in the SUPs) and pure alloy powder; see the red and black curves in Fig. 6a. Both spectra show their main absorbance band around 400 nm, and the absorbance of the NiAl alloy is ~110% higher than that of the Al layer. If the Ag NPs are deposited on the Al layer, the absorbance in the range of 200-700 nm is increased ~3.5 times, compare red and blue curves. A new broad band is observed around 385 nm, which matches the absorption of the Ag NPs utilized in this research; see their plasmon around 400 nm in Fig. S10 of the ESI.† If the NiAl alloy is deposited on the Al layer, the absorbance is increased ~4.5 times with respect to the red curve for the bare Al layer. When both the alloy and Ag NPs are present on the FSERS substrate, the absorbance is enhanced even more (up to 5.7 times with respect to the red curve); see the violet curve in Fig. 6a. This means that having both materials in the Al substrate favor the absorption of light in the visible region.

 

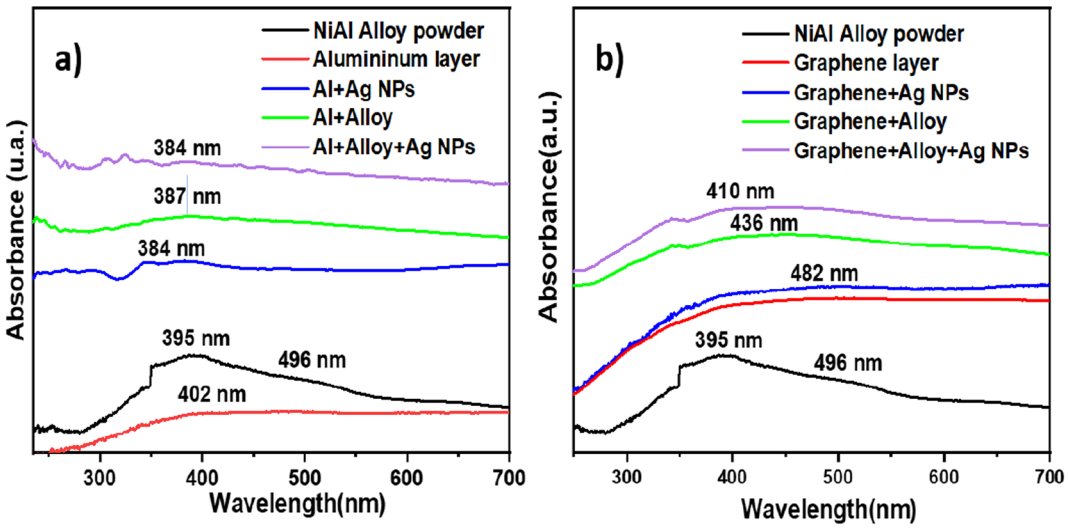


**Fig. 6** Optical absorbance spectra for (a) NiAl powder, Al layer, Al + alloy, Al + Ag-NPs and Al + alloy + Ag-NPs and (b) NiAl alloy, graphene substrate, G + alloy, G + Ag-NPs and G + alloy + Ag-NPs.

Similarly, adding NiAl alloy or Ag NPs to the graphene layer enhanced the absorbance with respect to the bare graphene, comparing the green and blue curves with the red line in Fig. 6b. Again, with both, the Ag NPs and the alloy on the graphene layer increased the absorbance of light to a maximum; see the violet curve in Fig. 6b. Then, we could infer from the absorbance spectra that the absorption of visible light at 532 nm is enhanced after adding the metal alloy or Ag NPs. This benefits the generation of Raman photons because the laser wavelength utilized to record the Raman spectra was 532 nm. Hence, the first reason for the maximum Raman enhancement observed in the FSERS substrates made with Al + alloy + Ag-NPs is the strong absorption of the laser at 532 nm. Another reason why our FSERS substrates (made with Al + alloy + Ag-NPs) have much more sensitivity for the detection of RhB (in comparison with previous works) is the formation of multiple conglomerates of Ag NPs on the SERS substrates. According to the literature, the intensity of the electric field (hotspot) between two spherical Ag NPs is enhanced by reducing the separation distance between them.[29] Furthermore, aggregates of spherical Ag NPs create multiple hotspots that increase the Raman signal.[2] In our case, the multiple Ag aggregates were formed on the Al substrates and NiAl alloy microparticles. Fig. S11a in the ESI† shows an SEM image of the bare NiAl alloy microparticles. Next, Fig. S11b† shows a zoomed view of the NiAl alloy microparticles decorated with Ag NPs (previously visualized in Fig. 1d). As observed in Fig. S11b,† the surface of the alloy is saturated with clusters of Ag NPs, and hundreds of Ag aggregates are observed. A closer view of the surface decorated with Ag NPs (Fig. S11c†) clearly shows the Ag aggregates formed by at least 10–30 Ag NPs; see the red circles. To confirm the formation of multiple hot spots in the agglomeration of Ag NPs, the COMSOL Multiphysics software was utilized to simulate the electric field among 10 Ag NPs with an average size of 10 nm and a separation distance of 2 nm. This last separation distance was selected because the RhB molecule has an average length and width of 1.6 and 1.1 nm, respectively.[30] Thus, the RhB molecule can be trapped among Ag NPs. The results of the simulation are depicted in Fig. S12a in the ESI.† As observed, all the nanoparticles interact strongly among themselves to form hotspots (see the red areas). Thus, the formation of Ag aggregates on the alloy microparticles was a critical factor in enhancing the number of hotspots on the FSERS made with Al + alloy + Ag-NPs. Another reason for the increased generation of Raman photons is the movement of electrons on the metallic surface of the NiAl alloy after the absorption of light from the green laser (532 nm). As depicted in Fig. 6a, the pure alloy strongly absorbs the green light (see extended band from 350 to 560 nm). If this occurs, free electrons located on the surface of the alloy microparticles move, generating an electric field that is summed (added) to the electric field of the electrons oscillating on the Ag NP surface. Then, the electric field (hotspot area) is amplified even more due to the contribution of the free electrons oscillating on the alloy's surface. This last effect is possible due to the high electronic density of NiAl.[31] Thus, coupling the electric field of the Ag NPs with that of the NiAl alloy drastically amplifies the generation of hotspots (even between the alloy's surface and the Ag NPs). To confirm the generation of hotspots among the alloy microparticles and the Ag NPs, the COMSOL software was utilized. The size of the alloy microparticle and Ag nanoparticle in the simulation was 1 μm and 10 nm, respectively. The separation distance among the particles was 2 nm. Fig. S12b† shows a zoomed view of the Ag NPs on the alloy microparticle. As observed, the electric field between the alloy's surface and the Ag nanoparticle is strong (see the red points). Thus, having agglomerations of Ag NPs on the alloy microparticles generates more hotspots, facilitating the detection of RhB molecules by the SERS effect. We believe that the detection of RhB molecules is more effective

when they are deposited on alloys decorated with Ag NPs. However, having the RhB molecules on the uncovered part of the FSERS substrate, that is, where we have only Al + Ag-NPs (see Fig. S2a†), is also effective for the detection of RhB because aggregates of Ag NPs formed by 3–12 nanoparticles are also present. Such aggregates are a source of multiple hotspots, as demonstrated previously.

If the EF values of the FSERS substrates made with the Al layer are compared with the FSERS substrates made of graphene, we observe that the highest Raman enhancement was obtained in the FSERS substrates made with the Al layer. This is due to the following reasons: (1) a higher amount of Ag-NP conglomerations was observed on the Al layer decorated with Ag NPs. Fig. 2c shows the aggregates of Ag NPs on the graphene sheets (FSERS made with G + Ag-NPs), which are much more separated in comparison with the Ag NP aggregates deposited on the Al layer (FSERS made with Al + Ag-NPs) (Fig. 1c). Due to the higher presence of aggregates on the Al layer, the formation of hotspots is much higher in this substrate than in the graphene substrate. Therefore, the limit of detection was two orders of magnitude lower in the FSERS substrates made with Al compared to the AAAg-8 and GAAg-7 samples in Tables S2 and S4 of ESI.† (2) The second reason for the higher enhancement factors in the FSERS substrates made with Al was the relative content of $Ag^0$ and $Ag^+$ species in that substrate. To determine the content of such Ag species on the FSERS substrates made with graphene and Al, XPS measurements were carried out for the Ag 3d orbital. Fig. 7a depicts the XPS spectrum corresponding to the FSERS substrate made of Al + Ag-NPs, and it exhibits deconvoluted bands associated exclusively with $Ag^0$ [32–34] and one satellite peak at 376.1 eV. All these last peaks are observed in the range of 365–380 eV. After adding the NiAl alloy microparticles to the FSERS substrate made of Al + Ag-NPs (to obtain the FSERS substrate made of Al + alloy + Ag-NPs), all the deconvoluted bands are displaced to the range of 362–375 eV (Fig. 7b). This shift of 5–6 eV toward lower energies is typically associated with physical interactions between the Ag NPs and a metallic surface[35,36] and the charging effect,[37] where free electrons of one metal disturb the ones located on the surface of silver nanoparticles.

A similar effect occurs for the FSERS substrate made with a graphene layer. Fig. 7c shows the XPS spectrum (Ag 3d orbital) for the FSERS substrate made of G + Ag-NPs, which exhibits deconvoluted bands attributed to $Ag^+$ and $Ag^0$ in the range of 367–377 eV. After adding the NiAl alloy microparticles to the FSERS substrate made of G + Ag-NPs (to obtain the FSERS substrate made of G + alloy + Ag-NPs), all the deconvoluted bands are displaced to the range of 362–374 eV (Fig. 7d). This shift is again attributed to the interaction of the Ag NPs and the alloy, which involves resonance that enhances the generation of Raman photons. It is worth mentioning that the FSERS substrates made of Al + Ag-NPs presented only metallic silver $Ag^0$ on their surface, while the FSERS made of G + Ag-NPs had approximately 65% $Ag^0$ and 35% $Ag^+$ (associated with $Ag_2O$). Thus, the higher EF values obtained in the FSERS substrates made with Al + Ag could be attributed to the higher content of Ag metal on it.

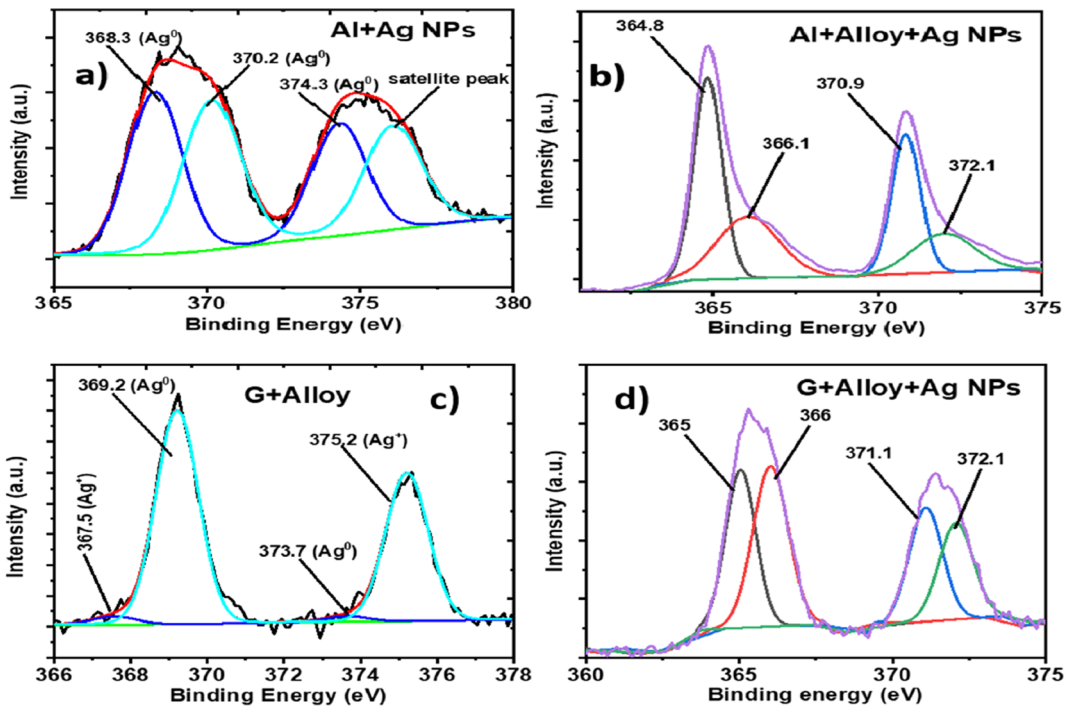


Fig. 7 XPS spectra for the Ag 3d orbital corresponding to the FERS substrates made of (a) Al + Ag-NPs, (b) Al + alloy + Ag-NPs, (c) G + Ag-NPs and (d) G + alloy + Ag-NPs.

## 4. Conclusions

We reported novel flexible SERS substrates fabricated with recycled plastics, which had a total area of 1 $cm^2$. We took advantage of the Al layer in wasted single-use packets to fabricate the FSERS substrates. They were employed to detect RhB, which is a toxic dye contaminant. The FSERS substrates made of Al + Ag-NPs had LOD and EF values of $8.35 \times 10^{-22}$ moles (~503 molecules) and $3.11 \times 10^{15}$, respectively. If NiAl alloy microparticles are added to the substrate made of Al + Ag-NPs, the LOD decreases to $8.35 \times 10^{-24}$ moles (~5 molecules) and the EF increases to $2.05 \times 10^{17}$. Similarly, FSERS substrates were made with graphene-layer + Ag-NPs or graphene-layer + NiAl-alloy + Ag-Nps. The best LOD and EF values of the substrates made with graphene were $8.35 \times 10^{-22}$ moles and $6.89 \times 10^{15}$, respectively. Thus, the FSERS substrates made with the Al layer have a higher sensitivity for the detection of RhB in comparison with those made with the graphene layer. The combination of Ag-NPs and NiAl alloy microparticles allowed the zeptomole detection of RhB for the following reasons: (1) the presence of the NiAl alloy on the substrate enhanced the absorption of the green light (laser of 532 nm) by ~4.5 times more with respect to the bare Al layer, which maximized the generation of Raman photons and (2) the surface of the metallic NiAl alloy had free electrons that oscillated after the interaction with the green laser. These electrons contributed to enhancing the local electric field among the Ag NPs, thereby increasing the number of hotspots for the detection of RhB. Furthermore, the FSERS substrates made with Al had higher EF values for the following reasons: (i) a higher presence of Ag aggregates was observed on the Al substrate in comparison with the graphene substrate, which produced a higher number of hotspots for the Raman enhancement and (ii) a higher content of $Ag^0$ (metallic silver) was found on the FSERS substrates made with Al + Alloy + Ag in comparison with the substrates made with graphene + alloy + Ag, which, in turn, maximized the generation of Raman photons by plasmonic effects. Basically, we presented here an inexpensive FSERS substrate, which does not require expensive materials, such as Si or Au films/Au-NPs, for the zeptomole detection of RhB as previously reported in the literature. Instead, we used wasted plastics and cheap alloy microparticles. Furthermore, the flexibility of our FSERS substrate allows its coupling to any curved surface for the detection of contaminants.

## Data availability

The data supporting this article have been included as part of the ESI.†

## Conflicts of interest

The authors declare no conflict of interest.

## Acknowledgements

Jorge Oliva thanks for the funding provided by Marcos Moshinsky Foundation. Authors also appreciate the support from LANOCAT laboratory as well as the technical help from A. Pena, B. Rivera and I. Becerril for XRD, Raman and SEM measurements.

## References

1 N. H. H. Hairom, C. F. Soon, R. M. S. R. Mohamed, M. Morsin, N. Zainal, N. Nayan, C. Z. Zulkifli and N. H. Harun, A review of nanotechnological applications to detect and control surface water pollution, *Environ. Technol. Innovation*, 2021, **24**, 102032.
2 P. C. Pinheiro, A. L. Daniel-da-Silva, H. I. S. Nogueira and T. Trindade, Functionalized Inorganic Nanoparticles for Magnetic Separation and SERS Detection of Water Pollutants, *Eur. J. Inorg. Chem.*, 2018, **2018**(30), 3443–3461.
3 D. Zhang, H. Pu, L. Huang and D. W. Sun, Advances in flexible surface-enhanced Raman scattering (SERS) substrates for nondestructive food detection: Fundamentals and recent applications, *Trends Food Sci. Technol.*, 2021, **109**, 690–701.
4 M. S. S. Bharati, V. R. Soma, M. S. S. Bharati and V. R. Soma, Flexible SERS substrates for hazardous materials detection: recent advances, *Opto-Electron. Adv.*, 2021, **4**(11), 210048.
5 L. Li and W. S. Chin, Rapid fabrication of a flexible and transparent Ag Nanocubes@PDMS film as a sers substrate with high performance, *ACS Appl. Mater. Interfaces*, 2020, **12**(33), 37538–37548.
6 A. (. Phelan, K. Meissner, J. Humphrey and H. Ross, Plastic pollution and packaging: Corporate commitments and actions from the food and beverage sector, *J. Cleaner Prod.*, 2022, **331**, 129827.
7 A. A. Al-Gheethi, Q. M. Azhar, P. S. Kumar, A. A. Yusuf, A. K. Al-Buriahi, R. M. S. R. Mohamed and M. M. Al-shaibani, Sustainable approaches for removing Rhodamine B dye using agricultural waste adsorbents: A review, *Chemosphere*, 2022, **287**, 132080.
8 D. Xu, Y. Zhang, S. Zhang, W. Yang, Z. Wang and J. Li, Copper nanoleaves SERS substrates with high surface roughness for sensitive detection crystal violet and rhodamine 6G, *Opt. Laser Technol.*, 2022, **145**, 107502.
9 L. Yang, J. Hu, L. He, J. Tang, Y. Zhou, J. Li and K. Ding, One-pot synthesis of multifunctional magnetic N-doped graphene composite for SERS detection, adsorption separation and photocatalytic degradation of Rhodamine 6G, *Chem. Eng. J.*, 2017, **327**, 694–704.
10 N. Sykam, N. D. Jayram and G. Mohan Rao, Exfoliation of graphite as flexible SERS substrate with high dye adsorption capacity for Rhodamine 6G, *Appl. Surf. Sci.*, 2019, **471**, 375–386.
11 S. Mao, F. Pei, S. Feng, Q. Hao, P. Zhang, Z. Tong, X. Mu, W. Lei and B. Liu, Detection of trace Rhodamine B using

stable, uniformity, and reusable SERS substrate based on Ag@$SiO_2$-Au nanoparticles, *Colloids Surf., A*, 2023, **657**, 130595.

12 Y. Zhao, G. Chen, Y. Du, J. Xu, S. Wu, Y. Qu and Y. Zhu, Plasmonic-enhanced Raman scattering of graphene on growth substrates and its application in SERS, *Nanoscale*, 2014, **6**(22), 13754–13760.

13 N. T. T. Phuong, T. X. Hoang, N. L. N. Tran, L. G. Phuc, V. D. Pung, H. K. T. Ta, T. N. Bach, N. H. T. Tran and K. T. L. Trinh, Rapid and sensitive detection of Rhodamine B in food using the plasmonic silver nanocube-based sensor as SERS active substrate, *Spectrochim. Acta, Part A*, 2021, **263**, 120179.

14 L. Pérez-Mayen, J. Oliva, A. Torres-Castro and E. De la Rosa, SERS substrates fabricated with star-like gold nanoparticles for zeptomole detection of analytes, *Nanoscale*, 2015, **7**(22), 10249–10258.

15 X. Dong, X. Ji, J. Jing, M. Li, J. Li and W. Yang, Synthesis of Triangular Silver Nanoprisms by Stepwise Reduction of Sodium Borohydride and Trisodium Citrate, *J. Phys. Chem. C*, 2010, **114**(5), 2070–2074.

16 S. T. Camagu, N. M. Mathabathe, D. E. Motaung, T. F. G. Muller, C. J. Arendse and A. S. Bolokang, Investigation into the thermal behaviour of the B2—NiAl intermetallic alloy produced by compaction and sintering of the elemental Ni and Al powders, *Vacuum*, 2019, **169**, 108919.

17 X. Xu, Z. Liu, B. Zhang, H. Chen, J. Zhang, T. Wang, K. Zhang, J. Zhang and P. Huang, Effect of Mn content on microstructure and properties of 6000 series aluminum alloy, *Appl. Phys. A: Mater. Sci. Process.*, 2019, **125**(8), 1–9.

18 Y. Meng, A sustainable approach to fabricating Ag nanoparticles/PVA hybrid nanofiber and its catalytic activity, *Nanomaterials*, 2015, **5**(2), 1124–1135.

19 H. Kaczmarek, M. Chylińska, B. Królikowski, E. Klimiec, D. Bajer and J. Kowalonek, Influence of glass beads filler and orientation process on piezoelectric properties of polyethylene composites, *J. Mater. Sci.: Mater. Electron.*, 2019, **30**(24), 21032–21047.

20 A. A. Muhsan and K. Lafdi, Numerical study of the electrochemical exfoliation of graphite, *SN Appl. Sci.*, 2019, **1**(3), 276.

21 C. Tan, X. Huang and H. Zhang, Synthesis and applications of graphene-based noble metal nanostructures, *Mater. Today*, 2013, **16**(1–2), 29–36.

22 S. Lin, W. L. J. Hasi, X. Lin, S. Han, X. Lou, F. Yang, D. Lin and Z. Lu, Rapid and sensitive SERS method for determination of Rhodamine B in chili powder with paper-based substrates, *Anal. Methods*, 2015, **7**(12), 5289–5294.

23 S. P. Godad and S. Kamal, Multifunctional Ag2CO3 microrods as SERS-active substrate for the detection and degradation of Rhodamine B dye, *Spectrochim. Acta, Part A*, 2021, **263**, 120176.

24 D. Xu, H. Jiang, S. Zhang, W. Yang, Y. Zhang, Z. Wang and J. Chen, High roughness gold nanoparticles/silver nanowires composites: Fabrication, characterization and ultrasensitive SERS detection towards Rhodamine B, *Microchem. J.*, 2020, **158**, 105136.

25 T. K. Naqvi, A. K. Srivastava, M. M. Kulkarni, A. M. Siddiqui and P. K. Dwivedi, Silver nanoparticles decorated reduced graphene oxide (rGO) SERS sensor for multiple analytes, *Appl. Surf. Sci.*, 2019, **478**, 887–895.

26 V. Moreno, K. Murtada, M. Zougagh and Á. Ríos, Analytical control of Rhodamine B by SERS using reduced graphene decorated with copper selenide, *Spectrochim. Acta, Part A*, 2019, **223**, 117302.

27 Y. Sun, W. Li, L. Zhao, F. Li, Y. Xie, W. Yao, W. Liu and Z. Lin, Simultaneous SERS detection of illegal food additives rhodamine B and basic orange II based on Au nanorod-incorporated melamine foam, *Food Chem.*, 2021, **357**, 129741.

28 M. Gómez, M. D. Murcia, R. Dams, N. Christofi, E. Gómez and J. L. Gómez, Removal efficiency and toxicity reduction of 4-chlorophenol with physical, chemical and biochemical methods, *Environ. Technol.*, 2012, **33**(9), 1055–1064.

29 S. Cortijo-Campos, R. Ramirez-Jimenez, E. Climent-Pascual, M. Agular-Pujol, F. Jimenez-Villacorta, L. Martinez, R. Jiménez-Riobóo, C. Prieto and A. de Andrés, Raman amplification in the ultra-small limit of Ag nanoparticles on $SiO_2$ and graphene: Size and inter-particle distance effects, *Mater. Des.*, 2020, **192**, 108702.

30 A. J. Bain, P. Chandna, G. Butcher and J. Bryant, Picosecond polarized fluorescence studies of anisotropic-fluid media. II. Experimental studies of molecular order and motion in jet aligned rhodamine 6G and resorufin solutions, *J. Chem. Phys.*, 2000, **112**, 10435.

31 Y. Cao, P. Zhu, J. Zhu and Y. Liu, First-principles study of NiAl alloyed with Co, *Comput. Mater. Sci.*, 2016, **111**, 34–40.

32 S. Das and T. L. Alford, Improved efficiency of P3HT:PCBM solar cells by incorporation of silver oxide interfacial layer, *J. Appl. Physiol.*, 2014, **116**(4), 044905.

33 A. K. Mohamedkhair, Q. A. Drmosh and Z. H. Yamani, Silver Nanoparticle-decorated tin oxide thin films: synthesis, characterization, and hydrogen gas sensing, *Front. Mater.*, 2019, **6**, 479759.

34 N. J. Firet, M. A. Blommaert, T. Burdyny, A. Venugopal, D. Bohra, A. Longo and W. A. Smith, Operando EXAFS study reveals presence of oxygen in oxide-derived silver catalysts for electrochemical $CO_2$ reduction, *J. Mater. Chem. A*, 2019, **7**(6), 2597–2607.

35 A. Dolatkhah, P. Jani and L. D. Wilson, Redox-Responsive Polymer Template as an Advanced Multifunctional Catalyst Support for Silver Nanoparticles, *Langmuir*, 2018, **34**, 10560.

36 Q. Cai, S. Mateti, W. Yang, R. Jones, K. Watanable, T. Taniguchi, S. Huang, Y. Chen and L. H. Li, Boron Nitride Nanosheets Improve Sensitivity and Reusability of Surface Enhanced Raman Spectroscopy, *Angew. Chem., Int. Ed.*, 2016, **55**, 8457.

37 X. Jing, H. Wang, H. Chen, J. Huang, Q. Li and D. Sun, Biosynthesized Ag/a-$Al_2O_3$ catalyst for ethylene epoxidation: the influence of silver precursors, *RSC Adv.*, 2014, **4**, 27597.

 